MIT Libraries | DSpace@MIT

MIT Open Access Articles

Ember: An open-source, transient solver for 1D reacting flow using large kinetic models, applied to strained extinction

The MIT Faculty has made this article openly available. ***Please share*** how this access benefits you. Your story matters.

Citation: Long, Alan E., Raymond L. Speth, and William H. Green. "Ember: An open-source, transient solver for 1D reacting flow using large kinetic models, applied to strained extinction." Combustion and Flame, 195 (September 2018): 105-116

As Published: http://dx.doi.org/10.1016/j.combustflame.2018.05.001

Publisher: Elsevier BV

Persistent URL: https://hdl.handle.net/1721.1/123991

Version: Author's final manuscript: final author's manuscript post peer review, without publisher's formatting or copy editing

Terms of use: Creative Commons Attribution-NonCommercial-NoDerivs License

Massachusetts Institute of Technology

Ember: An open-source, transient solver for 1D reacting flow using large kinetic models, applied to strained extinction.

Alan E. Long, Raymond L. Speth, William H. Green

Department of Chemical Engineering, Massachusetts Institute of Technology, 77 Massachusetts Ave., Cambridge, MA 02139, USA

Abstract

Simulation of quasi one-dimensional reacting flow is a standard in many combustion studies. Here Ember, a new open-source code for efficiently performing these calculations using large, detailed chemical kinetic models is presented. Ember outperforms other standard software, such as Chemkin, in computation time by leveraging rebalanced Strang operator splitting which does not suffer the steady-state inaccuracies of most splitting methods. The splitting approach and implementation used in Ember is described. Ember is validated for computation of flame extinction through imposed strain, extinction strain rate (ESR), and shown to be capable of modeling three typical experimental strained flame configurations: premixed twin flames, premixed single flames opposing inert, and diffusion flames. As further demonstration, Ember is used to investigate Lewis number effects on ESR using a detailed chemical kinetic model with 500 species for simulation of strained extinction of lean ($Le > 1$) and rich ($Le < 1$) propane/air flames. Primary trends predicted by Law [1] using asymptotic theories of strained flames are accurately reproduced with the large, detailed chemical kinetic model. However, the complicated chemistry introduces some subtle phenomena not seen with single-step models. The Ember software is open-source and freely available to any user online.

Keywords: Extinction Strain Rate, 1D Flames, Lewis Number

1. Introduction

Much of our understanding of combustion is derived from one-dimensional (1D) systems and models. Asymptotic analysis of flame models using simplistic chemistry has proven to be extremely useful in understanding a variety of combustion phenomena; examples include several key contributions by Law [1, 2]. One-dimensional numerical simulations of flat, cylindrically symmetric, or radially symmetric flames using detailed chemistry models are used to compute a variety of important fuel combustion properties including flame speeds, extinction strain rates, and to understand formation of pollutants by different fuels. They are also used in interpretation of flat flame data, including molecular beam mass spectrometry experiments. Often multiple 1D simulations need to be run, e.g., to build up or validate flamelet libraries, or to cover the range of flame conditions that will be encountered in a

Email address: whgreen@mit.edu (William H. Green)

combustion device. Accurate fuel chemistry models typically include hundreds of species and thousands of reactions, so fast, robust numerical solvers for 1D reacting flows are needed. Currently-available 1D flame solvers including Chemkin, Cantera, and FlameMaster rely on discretized axial domains and damped Newton methods [3–5]. This means that the system Jacobian bandwidth grows approximately linearly with number of species. However, computation time for factorization of the Jacobian (necessary when using direct Newton methods) scales according to the Jacobian bandwidth cubed [6], causing these solvers to slow down significantly as the number of species increases. By leveraging sparsity within the bandwidth, some improvement over this cubic scaling is attainable [7, 8]. New software tools implementing algorithms that scale better for large numbers of species are needed [9].

Extinction Strain Rate (ESR) has long been recognized as a particularly important flame property. Recent works have exposed new value in the realm of turbulent combustion for this fundamental flame parameter [10–12] which has been studied heavily by Law and co-workers [13–20]. In 2015, Shanbhogue et al. [10] observed that flame shape and instability were well characterized by the ESR of the combustion mixture in the case of turbulent, swirl-stabilized, premixed CH_4/H_2 combustion. These flames were studied at constant Reynolds number and swirl angle. A subsequent paper expands this analysis to varying Reynolds numbers and swirl angles through use of a modified Karlovitz number, defined as the ratio of the outer recirculation zone (ORZ) frequency to the mixture ESR at the point the flame expands into the ORZ. The modified Karlovitz number used was found to be constant for the swirled, turbulent, methane flames studied. This observation was consistent for varying hydrogen percentage as well [11]. The two works, while constrained to methane based fuel mixtures, suggest that ESR plays a critical role in determining the extent and edge behavior of turbulent flames. A third study further highlights the significance of ESR for turbulent flames by examining such flames stabilized by flow around a bluff body. The work finds that the flame offset distance from the bluff body correlates with the ESR value of the fuel/oxidizer mixture. This study again focuses on CH_4/H_2 flames [12].

Law's early work on flame extinction focused on systems involving droplet vaporization leading to diffusion flames where asymptotic analyses were employed [2, 13]. In a series of experimental works, Law and coworkers detailed extinction of propane/air mixtures in both stagnation flow against a smooth surface and in opposed axisymmetric jet flow [14, 15, 21]. The first work observed the importance of velocity gradient, strain, in governing flame extinction [21]. The second and third works investigated the impact of downstream heat-loss and preferential diffusion on the extinction of premixed flames by using both impinging jets and stagnation flow against a surface. The work found downstream heat loss and/or incomplete combustion, rather than stretch alone, to be necessary to achieve extinction for fuel mixtures in which the deficient reactant had a larger diffusion rate [14]. Additionally, it was observed that flame-front instability due to preferential diffusion occurred only under rich conditions for the propane/air mixtures studied [15]. A numerical study examining high-stretch extinction limits by Law and coworkers concludes that radiative losses have little impact on ESR [16]. A 1986 paper by Law et al. provided the first full experimental characterization of ESR as a function of equivalence ratio, doing so for twin/double, impinging, premixed methane and propane flames [17]. In a subsequent work, the importance of Lewis number with regard to flame extinction was demonstrated [22]. Law and coworkers also produced several works on non-steady extinction effects by sinusoidal variations in opposed jet velocities. For high

oscillation frequencies, it was shown that the steady ESR might be surpassed without extinction if a more favorable strain rate is once again imposed in a time scale sorter than that of extinction, confirming that extinction is not an instantaneous process [19]. This observation was later expanded to strained premixed flames [23, 24] and to oscillations in the context of spherical flame extinction [25, 26].

Further efforts in calculation and measurement of ESR have been made by Egolfopoulos and coworkers, one of Law's former students. These efforts have expanded ESR characterization across a wide range of fuels including, ethanol [27], dimethyl ether [27, 28], C5-C12 alkanes [29], cyclopentadiene [30], JP-5 [31], and more [32–35]. Many other significant efforts toward expanding the ESR database have been made by Niemann and coworkers [36–43] and other researchers [44–48]. Some recent works have begun to experimentally characterize ESR at elevated pressures thanks to new, enclosed counterflow apparatuses and refined seeding procedures [35, 42, 48].

Current computations of ESR typically rely on the use of the Chemkin software suite first published by Robert Kee and coworkers in 1980 and later expanded to include a module for the calculation of ESR [49–51]. The ESR computation module in Chemkin is based on a 1988 article by Kee et al. which developed the boundary value formulation for 1D axisymmetric opposed jet reacting flow. The plug flow boundary value problem (BVP) formulation published by Kee et al. [52] offered significantly improved agreement with experimental measurements of ESR when compared with previous formulations which assumed infinitely separated jets producing purely potential flow. This formulation was later extended by Nishioka, Law, and Takeno through the introduction of internal temperature boundary conditions which allow for traversing the extinction turning point of the flame S-curve through pseudo-arclength continuation preventing the Jacobian of the numerical system from becoming singular at the extinction point [20]. This method has since been added to the Chemkin ESR module [3]. The Nishioka et al. method works well for many smaller kinetic models, and has been used in several recent works for comparisons with experimental results [29, 53]. Unfortunately, the Nishioka et al. method implemented in Chemkin takes prohibitively long when attempting to run calculations for larger more detailed mechanisms, even when using the ChemkinPro solver which takes advantage of Jacobian sparsity (Figure 6b). At the same time, many modern kinetic model production efforts are aimed at producing more complete models for increasingly complex fuels and fuel blends [40, 54]. For example, models from NUI Galway, AramcoMech1.3 and AramcoMech2.0, which seek to characterize C1-C4 chemistry, possess 253 and 493 species respectively [55–61]. Furthermore, current automated model generation techniques such as the Reaction Mechanism Generator (RMG) also produce kinetic models with large numbers of species [62, 63].

In this work, we introduce Ember, a new, freely-available, open-source code for the simulation of dynamic, 1D strained flames which, among other capabilities including laminar and strained flame speeds, provides superior performance for simulation of extinction strain rate with large kinetic models [64]. The code is C++ based for computational efficiency and wrapped in Python for convenience. It achieves improved performance by using rebalanced Strang splitting to reformulate the system into more efficiently solvable ODEs [65]. Further details are discussed in the Methods section of this work. The source code is available to the community on GitHub (`https://github.com/speth/ember`) under the MIT License, and a set of installation instructions and a dependency list are available in the documentation linked

to from GitHub. To demonstrate the new simulation capabilities available using Ember, the time-dependent solver is used to investigate artificial perturbations in Lewis number and track the impact on the flame, as well as calculating ESR for rich propane flames using a large, detailed mechanism. Progression to extinction is examined for $Le > 1$ and $Le < 1$.

2. Methods

The governing equations solved by Ember are for a time-dependent, strained, 1D flame with the strain rate imposed as a function of time. We introduce a unified formulation which permits the solution of planar, disc, and cylindrical flames, as depicted in Figure 1. In this section, we describe the governing equations for the flame, the spatial and temporal discretization schemes, and the numerical methods used to describe the discretized equations.

2.1. Governing Equations

The governing equations used here are based on the general forms derived by Kee et al. [66]. A unified formulation for the different strained flame geometries can be developed by introducing two parameters, α and β, where $\alpha = 0$ for planar and disc flames and $\alpha = 1$ for cylindrical flames, and $\beta = 1$ for planar and cylindrical flames and $\beta = 2$ for disc flames. The coordinate and velocity normal to the flame are denoted x and v, respectively and the coordinate and velocity tangential to the flame (in which the flame is stretched) are denoted z and u, respectively. The potential flow velocity field in the nonreacting flow (designated with the subscript ∞) can be written as

$$u_\infty = \frac{az}{\beta}; \qquad v_\infty = \frac{a}{\alpha+1}\left(\frac{|R_s|R_s^\alpha}{x^\alpha} - x\right) \tag{1}$$

where a is the time-varying strain rate. In the case of the cylindrical flame, the constant R_s represents a line source/sink at the axis of symmetry that allows the stagnation surface to be a cylinder of radius R_s (which may be negative), permitting simulation of flames with arbitrary curvature. The stretch rate κ for a flame at radius R_f is

$$\kappa = a + \frac{\alpha}{R_f}\frac{dR_f}{dt} \tag{2}$$

When the flame is stationary, the stretch rate reduces to $\kappa = a$ and thus curvature does not contribute to the stretch rate for stationary flames in this configuration.

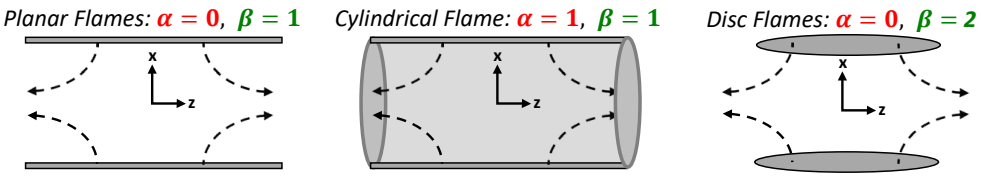

Figure 1: Strained flame configurations simulated by Ember.

The governing equation for momentum in the z-direction can be written, after removing terms that are either identically zero or neglected by the boundary layer approximation, as

$$\rho\frac{\partial u}{\partial t}+\rho u\frac{\partial u}{\partial z}+\rho v\frac{\partial u}{\partial x}=-\frac{\partial p}{\partial z}+\frac{1}{x^{\alpha}}\frac{\partial}{\partial x}\left[x^{\alpha}\mu\frac{\partial u}{\partial x}\right] \tag{3}$$

The pressure gradient outside the boundary layer can be found by substituting Equation 1 into Equation 3

$$\frac{\partial p}{\partial z}=-\frac{\rho_{\infty}z}{\beta}\frac{da}{dt}+\frac{\rho_{\infty}a^{2}z}{\beta^{2}} \tag{4}$$

where ρ_{∞} is the density of the unburned mixture. Introducing the notation $U\equiv ua/(\beta u_{\infty})=u/z$, substituting Equation 4 into Equation 3, and dividing by z, we obtain the momentum equation along the stagnation streamline

$$\rho\frac{\partial U}{\partial t}+\rho U^{2}+\rho v\frac{\partial U}{\partial x}=\frac{\rho_{\infty}}{\beta}\frac{da}{dt}+\frac{\rho_{\infty}}{\beta^{2}}a^{2}+\frac{1}{x^{\alpha}}\frac{\partial}{\partial x}\left[x^{\alpha}\mu\frac{\partial U}{\partial x}\right] \tag{5}$$

The mass continuity equation can be written as

$$\frac{\partial\rho}{\partial t}+\frac{1}{x^{\alpha}}\frac{\partial}{\partial x}\left(x^{\alpha}\rho v\right)+\frac{\partial(\rho u)}{\partial z}=0 \tag{6}$$

With the substitution for U, this becomes

$$\frac{\partial\rho}{\partial t}+\frac{1}{x^{\alpha}}\frac{\partial}{\partial x}\left(x^{\alpha}\rho v\right)+\beta\rho U=0 \tag{7}$$

The conservation equations for the species mass fractions Y_k are written as

$$\rho\frac{\partial Y_k}{\partial t}+\rho v\frac{\partial Y_k}{\partial x}=-\frac{1}{x^{\alpha}}\frac{\partial}{\partial x}\left[x^{\alpha}j_k\right]+\dot{\omega}_k W_k \tag{8}$$

where $\dot{\omega}_k$ are the molar production rates, W_k are the molecular weights. j_k are the diffusive mass fluxes, calculated as

$$j_k=-\rho D_{km}\frac{\partial Y_k}{\partial x}-\frac{D_k^T}{T}\frac{\partial T}{\partial x}+Y_k j' \tag{9}$$

where D_{km} are the mixture averaged diffusion coefficients relating mass fluxes to mass fraction gradients, D_k^T are the thermal diffusion coefficients (included when the multicomponent transport model is enabled), and j' is a correction term defined to enforce the requirement $\sum j_k=0$. We find j' by first calculating the uncorrected fluxes j_k^* using Equation 9 with $j'=0$ and then calculating $j'=-\sum j_k^*$.

The energy conservation equation is written neglecting compressibility and viscous effects. Along the stagnation streamline, the energy equation can then be written in terms of the temperature as

$$\rho\frac{\partial T}{\partial t}+\rho v\frac{\partial T}{\partial x}+\frac{1}{c_p}\sum_{k=1}^{K}\hat{h}_k\dot{\omega}_k+\frac{1}{c_p}\sum_{k=1}^{K}j_k c_{p,k}\frac{\partial T}{\partial x}=\frac{1}{c_p}\frac{1}{x^{\alpha}}\frac{\partial}{\partial x}\left[x^{\alpha}\lambda\frac{\partial T}{\partial x}\right] \tag{10}$$

where c_p is the mixture specific heat capacity, $\hat{h}_k$ are the species molar enthalpies, $c_{p,k}$ are the species specific heat capacities, and λ is the mixture thermal conductivity.

2.2. Spatial & Temporal Discretization

Equations 5, 7, 8, and 10 comprise the governing equations for the strained flame. These equations are spatially discretized on an adaptive one-dimensional grid, using first-order upwinded differences for convective terms, and second-order differences for other spatial derivatives. This produces a system of ODEs for T, U and Y_k with an algebraic constraint imposed by v. Boundary values or zero-gradient conditions are applied to T, U, and Y_k at each end of the domain, and the value of v is specified at one point (which may be internal to the domain). To simulate unstrained laminar flames, an internal fixed temperature condition is applied and used to calculate v at that point.

To efficiently integrate the governing equations in time, we employ the rebalanced splitting method [65] so that reaction, diffusion, and convection terms can be integrated separately. The rebalanced splitting method is applied recursively, first splitting the reaction and transport operators and then splitting the convection and diffusion operators within the transport operator. In order to make the split equations easy to integrate in parallel, we also split terms which couple multiple solution components at multiple grid points as a separate "cross" term. We denote the balanced reaction, diffusion, and convection operators as R^*, D^*, and C^*, respectively; the corresponding splitting constants as $\tilde{R}$, $\tilde{D}$, and $\tilde{C}$; the cross operator as X; and the components associated with the energy, species, and momentum equations with the subscripts T, Y_k, and U, respectively. The split governing equations may now be written as

$$\frac{\partial T}{\partial t} = R^*_T + C^*_T + D^*_T + X_T \tag{11}$$

$$\frac{\partial Y_k}{\partial t} = R^*_{Y_k} + C^*_{Y_k} + D^*_{Y_k} + X_{Y_k} \tag{12}$$

$$\frac{\partial U}{\partial t} = C^*_U + D^*_U \tag{13}$$

where the individual split terms are

$$R_T^* = -\frac{1}{\rho c_p}\sum_{k=1}^{K}\hat{h}_k\dot{\omega}_k + \tilde{R}_T \tag{14}$$

$$R_{Y_k}^* = \frac{\dot{\omega}_k W_k}{\rho} + \tilde{R}_{Y_k} \tag{15}$$

$$C_T^* = -v\frac{\partial T}{\partial x} + \tilde{C}_T \tag{16}$$

$$C_{Y_k}^* = -v\frac{\partial Y_k}{\partial x} + \tilde{C}_{Y_k} \tag{17}$$

$$C_U^* = -U^2 - v\frac{\partial U}{\partial x} + \frac{\rho_\infty}{\rho\beta}\frac{da}{dt} + \frac{\rho_\infty}{\rho\beta^2}a^2 + \tilde{C}_U \tag{18}$$

$$D_T^* = \frac{1}{\rho c_p x^\alpha}\frac{\partial}{\partial x}\left[x^\alpha\lambda\frac{\partial T}{\partial x}\right] + \tilde{D}_T \tag{19}$$

$$D_{Y_k}^* = \frac{1}{\rho x^\alpha}\frac{\partial}{\partial x}\left[x^\alpha\rho D_{km}\frac{\partial Y_k}{\partial x}\right] + \tilde{D}_{Y_k} \tag{20}$$

$$D_U^* = \frac{1}{\rho x^\alpha}\frac{\partial}{\partial x}\left[x^\alpha\mu\frac{\partial U}{\partial x}\right] + \tilde{D}_U \tag{21}$$

$$X_T = \frac{1}{\rho c_p}\sum_{k=1}^{K} j_k c_{p,k}\frac{\partial T}{\partial x} \tag{22}$$

$$X_{Y_k} = \frac{1}{\rho x^\alpha}\frac{\partial}{\partial x}\left[x^\alpha\left(\frac{D_k^T}{T}\frac{\partial T}{\partial x} - Y_k j'\right)\right] \tag{23}$$

The integration of the system state vector y_n over a "global" timestep h to find y_{n+1} is performed by integrating the following ODEs starting at time t_n with $\xi_1, \ldots, \xi_7$ representing the intermediate states of the split solver

$$\frac{d\xi_1}{dt} = D^*\left(\xi_1\right); \quad \xi_1(t_n) = y_n \tag{24}$$

$$\frac{d\xi_2}{dt} = C^*\left(\xi_2\right); \quad \xi_2(t_n) = \xi_1(t_n + h/4) \tag{25}$$

$$\frac{d\xi_3}{dt} = D^*(z_3); \quad \xi_3(t_n + h/4) = \xi_2(t_n + h/2) \tag{26}$$

$$\frac{d\xi_4}{dt} = R^*(z_4); \quad \xi_4(t_n) = \xi_3(t_n + h/2) \tag{27}$$

$$\frac{d\xi_5}{dt} = D^*(z_5); \quad \xi_5(t_n + h/2) = \xi_4(t_n + h) \tag{28}$$

$$\frac{d\xi_6}{dt} = C^*(z_6); \quad \xi_6(t_n + h/2) = \xi_5(t_n + 3h/4) \tag{29}$$

$$\frac{d\xi_7}{dt} = D^*(z_7); \quad \xi_7(t_n + 3h/4) = \xi_6(t_n + h) \tag{30}$$

$$y_{n+1} = \xi_7(t_n + h) \tag{31}$$

To compute the splitting constants for the next timestep, we first calculate the following quantities, which can be thought of as average estimates of the reaction, convection, and

diffusion terms over the global timestep

$$R^{**} = \frac{1}{h}\left(\xi_4\Big|_{t_n}^{t_n+h}\right) - \tilde{R} \tag{32}$$

$$C^{**} = \frac{1}{h}\left(\xi_2\Big|_{t_n}^{t_n+h/2} + \xi_6\Big|_{t_n+h/2}^{t_n+h}\right) - \tilde{C} \tag{33}$$

$$D^{**} = \frac{1}{h}\left(\xi_1\Big|_{t_n}^{t_n+h/4} + \xi_3\Big|_{t_n+h/4}^{t_n+h/2} + \xi_5\Big|_{t_n+h/2}^{t_n+3h/4} + \xi_7\Big|_{t_n+3h/4}^{t_n+h}\right) - \tilde{D} \tag{34}$$

where the notation $\xi_i|_a^b$ indicates the difference $\xi_i(b) - \xi_i(a)$. The split constants to be used for the next timestep are then computed as

$$\tilde{R} = -\tfrac{1}{2}R^{**} + \tfrac{1}{2}C^{**} + \tfrac{1}{2}D^{**} + \tfrac{1}{2}X \tag{35}$$

$$\tilde{C} = \tfrac{1}{4}R^{**} - \tfrac{3}{4}C^{**} + \tfrac{1}{4}D^{**} + \tfrac{1}{4}X \tag{36}$$

$$\tilde{D} = \tfrac{1}{4}R^{**} + \tfrac{1}{4}C^{**} - \tfrac{1}{4}D^{**} + \tfrac{1}{4}X \tag{37}$$

2.3. Integration of the Split Equations

The reaction terms, Equations 14 and 15, are independent at each grid point, and thus are integrated separately and in parallel. The equations at each grid point are integrated using either the CVODE [67] which implements the backward differentiation formulas (BDF), or the CHEMEQ2 solver which implements a quasi-steady-state (QSS) algorithm [68]. The latter solver is of note because it does not rely on constructing and factorizing the system Jacobian, thus avoiding the $\mathcal{O}(K^3)$ scaling associated with fully implicit methods.

The convection terms, Equations 16, 17, and 18, are integrated together with the continuity equation 7. The time derivative of the density appearing in the continuity equation is evaluated at the start of each global timestep based on the values of R^{**}, C^{**}, and D^{**}. As written, these equations are all coupled by the density. We can eliminate this coupling by first using the ideal gas law to replace the density, $\rho = p\overline{W}/(\overline{R}T)$ where $\overline{W}$ is the mixture molecular weight and $\overline{R}$ is the molar gas constant. The mixture molecular weight is defined as

$$\frac{1}{\overline{W}} = \sum \frac{Y_k}{W_k} \tag{38}$$

Differentiating this with respect to time yields

$$\frac{\partial \overline{W}}{\partial t} = -\overline{W}^2 \sum \frac{1}{W_k}\frac{\partial Y_k}{\partial t} \tag{39}$$

Replacing $\partial Y_k/\partial t$ with Equation 17 yields a conservation equation for $\overline{W}$

$$\frac{\partial \overline{W}}{\partial t} = -v\frac{\partial \overline{W}}{\partial x} - \overline{W}^2 \sum \frac{\tilde{C}_{Y_k}}{W_k} \tag{40}$$

Equations 7, 16, 18, and 40 then form a complete system which may be integrated over a split timestep by first calculating v using Equation 7 given values for T, U, and $\overline{W}$, followed by evaluating the time derivatives for the latter three variables. This system of equations is not stiff, and so are integrated using the Adams-Moulton formulas as implemented by CVODE

[67]. Once the values of v have been calculated for the split timestep, the individual species equations can be integrated independently and in parallel according to Equation 17.

Assuming the mixture transport properties to be constant during each global timestep, the diffusion terms for each solution component are independent and can be integrated in parallel. This assumption also means that the ODE for each component is linear with constant coefficients, allowing a straightforward implementation of the second-order BDF integrator to be used.

Since the contributions from the cross terms X are small, these terms are calculated at the start of each global time-step and held constant through the split integration stages.

Thermodynamic, transport, and kinetic parameters needed in each equation are computed using Cantera [4]. We modify the normal rules for computing the mixture-averaged diffusion coefficients and viscosity to eliminate the $\mathcal{O}(K^2)$ scaling that these calculations usually entail. To do this, we apply a threshold condition on the species mole fractions X_k and include the contributions of species k on these mixture-averaged properties if $X_k > 10^{-5}$. This approximation has negligible impact on the accuracy of the solutions, but can reduce computational time significantly for large mechanisms.

In summary, Ember outperforms conventional solvers principally by solving time dependent solution using rebalanced Strang splitting to avoid a large stiff Jacobian and allowing for the stiff chemistry integrations to be performed in parallel, separately at each grid point, and using the significantly more efficient QSS method. The species diffusion integrations are also performed in parallel, separately for each species. The remaining convection terms are decoupled and integrated in parallel by introducing a surrogate transport equation for the mixture molecular weight. By separating integration of the reaction, diffusion, and convection terms, Ember is a good candidate for implementing further improvements in computation time through use of GPU processing or other algorithmic improvements that can be applied to any of the individual problems, rather than being limited to methods that can be applied to the coupled reacting flow problem. As an open-source code, Ember is also amenable to extensions from the community to enable other flame configurations where 1D approximations hold, such as transient, spherically expanding flames and the finite separation distance burner.

3. Results & Discussion

As a first step in validation of Ember for ESR calculations a comparison is made between strain progression curves to extinction points calculated by both Chemkin and Ember. A characteristic comparison is shown in Figure 2 for a premixed, lean, methane, twin flame extinction. Excellent agreement is observed between Chemkin ($ESR = 987s^{-1}$) and Ember ($ESR = 990s^{-1}$). The QSS integrator and approximate transport methods are observed to have negligible impact on accuracy. ESR for the Chemkin simulation is determined as the maximum of $|\frac{dv_{axial}}{dz}|$ before the flame using the pseudo arclength continuation method of Nishioka et al. [20] to traverse and identify the maximal strain rate turning point. For Ember, ESR is characterized as the maximum value of the strain parameter, a, that yields a burning solution. Adaptive step sizes for a are used in progressing to extinction. A minimum increase factor of 1.00001 is specified. Initially this may appear an unexpected result since, as discussed in the Methods section of this work, Ember employs a potential flow, or infinitely

separated opposed jets, formulation of the 1D reacting flow while Chemkin uses the fixed BVP formulation from Kee et al. [52]. However, in this case, the Chemkin simulation has been calculated for a large opposed flow burner separation distance (BSD) (5 cm) allowing it to behave nearly equivalently to the potential flow formulation [69].

Ember successfully computes all three types of flames typically considered in extinction studies, namely twin premixed flames, single premixed flames opposing an inert, and diffusion flames. Figure 3 shows Ember simulations for these three flame types at consistent strains of 300 s^{-1}. The premixed flames are computed using a stoichiometric equivalence ratio. Note that the stagnation plane is set at $x = 0$ and the twin flame simulation makes use of the symmetry of the domain. In this comparison, it is clear how the single flame system leads to lower extinction strain rates when compared with twin premixed flames since thermal energy diffuses into the inert opposing jet, thus reducing the strength of the flame. The twin flame achieves a peak temperature of 2170 K while the single flame peaks at $2060K$. With a fuel jet of pure methane, the diffusion flame produces the lowest maximum temperature at $1900K$. Following the general trend of peak flame temperature, Ember calculates the ESR values of these three conditions to be $1920s^{-1}$ for twin flames, $590s^{-1}$ for the single flame, and $480s^{-1}$ for the diffusion flame. The drastic reduction in ESR caused by using an inert opposed flow is often practically necessary from an experimental point of view to prevent turbulence and maintain laminar opposed flow since high initial flow velocities are required to impose high strains.

To assess the magnitude of computational improvement attained by the Ember, a set of strained flame computations were performed for methane flames using a selection of well-established kinetic models of varying sizes, Table 1. Due to solver issues (for both Em-

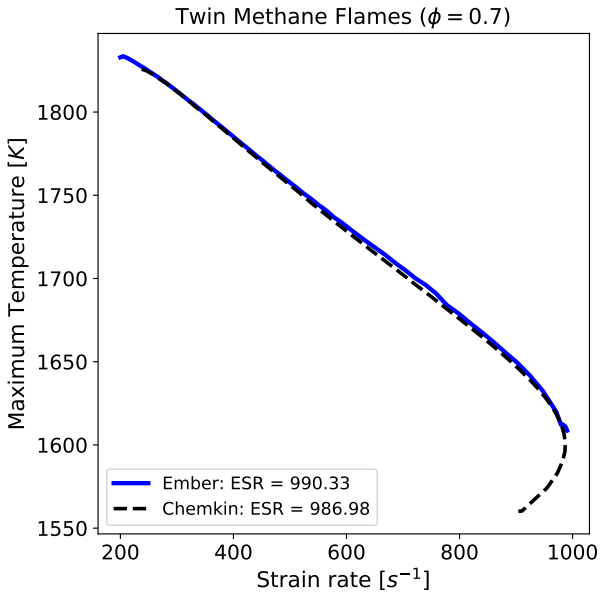

Figure 2: Comparison of extinction profiles generated using Ember and Chemkin for twin methane flames at an equivalence ratio of 0.7 using the Stanford FFCM1 kinetic model [70]. A BSD of 5 cm is used in Chemkin to approximate the infinitely separated potential flow formulation used in Ember. QSS chemistry integration and approximate transport methods are used.

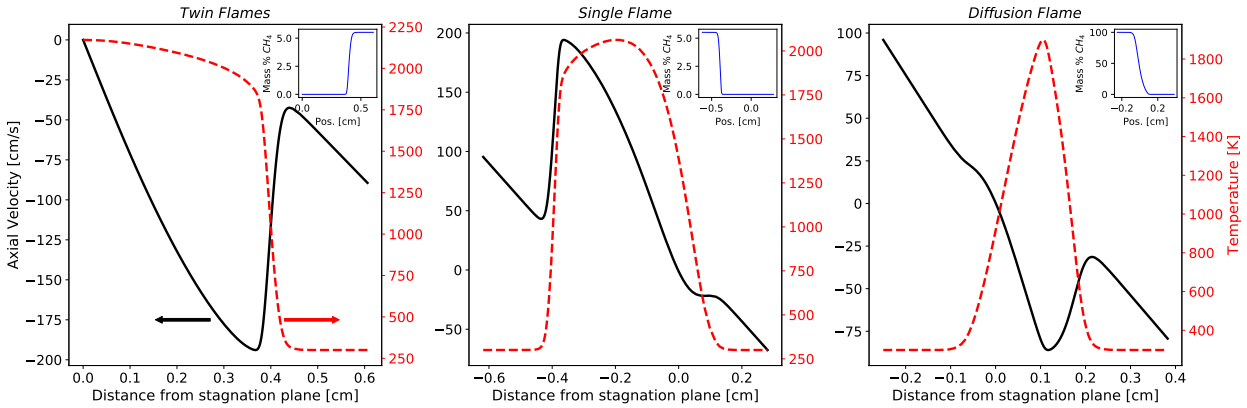

Figure 3: Characteristic flame types used for studying extinction phenomena. Simulations for strains set at $300s^{-1}$ on the flame side of the stagnation plane. Stoichiometric equivalence ratios used for single and twin flames. Opposed flow is nitrogen at room temperature for the single premixed flame. Pure methane opposes air for the diffusion flame.

ber and Chemkin) caused by reactions with unphysical reverse rates at low temperatures [71], the reaction `IC4H9O2+C2H4⇌IC4H9O2H+C2H3` is removed from AramcoMech 1.3 and `4C3H2(S)+M⇌C3H2+M`, `C4H71-3+C2H3COCH3⇌C8H131-5,3,TAO`, and `C4H63,1-2OH⇌C4H612+OH` are removed from AramcoMech 2.0. As a characteristic test case, a lean ($\phi = 0.7$) twin methane flame arrangement at standard temperature and pressure for the unburned gas and a strain rate of 500 s^{-1} is used. For adaptive griding, the Chemkin default parameters are used, 0.1 for gradient and 0.5 for curvature based re-griding. The parallel performance of Ember is shown in Figure 4. Ideal parallelism would yield an inverse dependence on the number of cores used since each additional core could perfectly share the computational load. This corresponds to a parallel efficiency of 1 as depicted in Figure 4. However, because Ember is only parallelizable down to the grid point for chemistry integrations and requires integration in series for each split step, some deviation ideal behavior is expected. Next, Figure 5 demonstrates the value of using rebalanced Strang splitting as opposed to traditional Strang splitting. The principal benefit of ensuring convergence to the correct steady state is clear, but as an additional benefit, rebalanced splitting is observed to yield significantly improved computation time. This is attributed to the large steady state offset in the case of traditional Strang splitting which in turn requires more computationally intensive sub-steps as the system continually overshoots the true steady state value. The default global step size in Ember is 20 μs and is used for all other Ember calculations.

In Figure 6, Ember computation times are compared with those of Chemkin. For these calculations, Chemkin-Pro 17.0 [72] is used and all calculations are constrained to parallelization over four CPUs. For Figure 6b the ESR computation time is scaled to the strain rate range of $500s^{-1}$ to $1000s^{-1}$. Computation times are fit to number of species power laws of the form $y = Ax^b$. The power law fitting is based on the factorization of the Jacobian, which scales according to dimension cubed for a dense matrix or bandwidth for a sparse matrix. Figure 6a additionally compares the computation time impacts of applying the QSS chemistry integrator and the transport approximation discussed in the Methods section. The most dramatic increase in efficiency comes from the implementation of the QSS chemistry

Table 1: Combustion kinetic models used for Ember computation speed evaluation.

Model	# Species	# Reactions	Reference
FFCM1	38	278	[70]
GRI3.0	53	325	[73]
USCII	111	784	[74]
AramcoMech1.3	253	1542	[55]
AramcoMech2.0	493	2716	[56–61]

method. When using the internal boundary condition formulation for progression to extinction in Chemkin, the ESR computation time points are observed scale approximately according as species cubed. The data point for AramcoMech 2.0 has been extrapolated to the set ESR range used in Figure 6 from a partial progression to extinction. This is a significant loss in computational efficiency when compared to the boundary velocity formulation (Fig. 6a) where Chemkin computation times are observed to scale with number of species squared. This suggests that sparse linear algebra methods have been implemented when solving the velocity boundary condition routine, but not for the internal temperature boundary condition routine used in the ESR module. Ember on the other hand, maintains nearly the same ideal scaling observed when computing the test flame at a strain rate of 500 s^{-1}, (species$^{1.2}$).

Analysis of stretched and strained flames in the literature often focuses on the impact of Lewis number, the dimensionless number expressing the ratio of the energy conduction

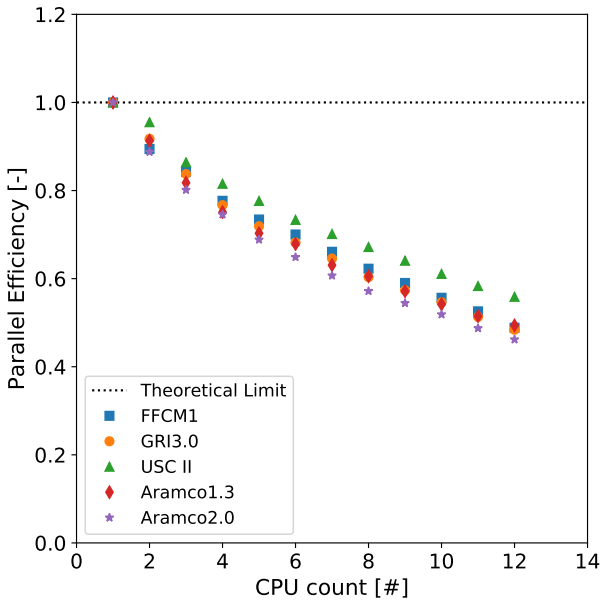

Figure 4: Parallel efficiency (single CPU time / n-CPU time / n) plotted against number of physical CPUs used to observe the parallel performance of Ember. Perfect parallelism would yield a constant value of 1 as the computational load is evenly spread over the available CPUs. QSS chemistry solver and the transport approximation method are used.

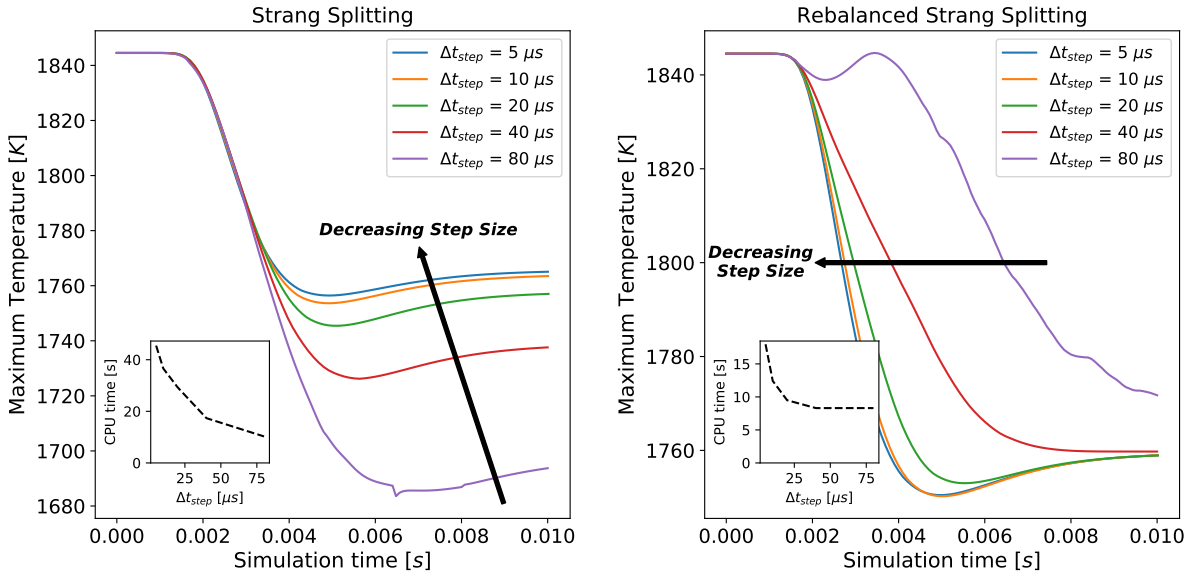

Figure 5: Methane twin disc flames. $\phi = 0.7$. Initial temperature 298K, atmospheric pressure. Comparison of simulation performance of rebalanced Strang splitting with traditional Strang splitting for varying global integration step sizes. Inset axes show total computation run times for each of the global steps using both methods.

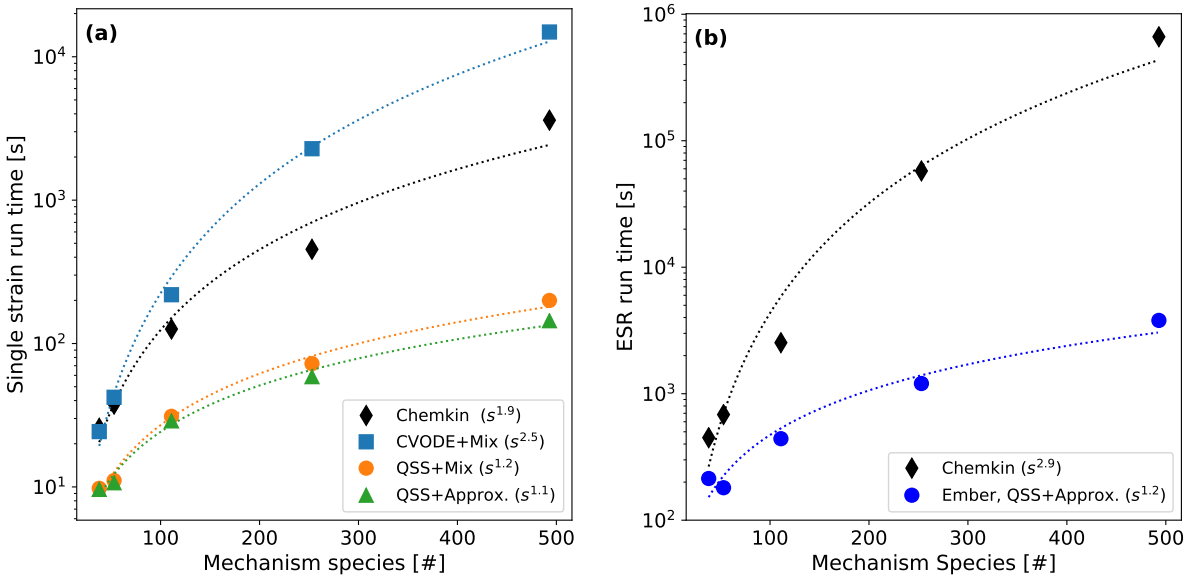

Figure 6: Methane twin disc flames. $\phi = 0.7$. Initial temp. 298K, atmospheric pressure. Parallelized over 4 CPUs. Fit to $t = As^B$ where t is time and s is number of species. (a) Computation times for a strain rate of 500 s^{-1} demonstrating the performance of Ember compared with Chemkin and the benefits of implementing the QSS chemistry integrator and mixture averaged transport approximation. (b) Comparison of Ember and Chemkin ESR computation times for varying kinetic model sizes.

rate to the species diffusion rate typically characterized using the diffusivity of the limiting reactant [1, 15]. Here the newly available time dependent solve capabilities of Ember are leveraged for an investigation into the impact of Lewis number limit behavior on strained flames. This is achieved using twin methane flames simulated at a strain rate of $500s^{-1}$ and systematically and instantaneously perturbing thermal conductivity, λ, or individual species diffusion coefficients, artificially forcing the Lewis number to extremes. The diffusion coefficients are modified within Ember such that the mixture averaged values are calculated normally and then the diffusion coefficient for the species of interest is set to 0. The FFCM1 kinetic model is used for this analysis [70]. A summary of these results for lean, stoichiometric, and rich conditions is shown in Figure 7. Since Ember is a transient solver, the convergence to the new steady state in each subplot is shown as a time progression from the initial steady state where all diffusion parameters have their normal value before the given diffusion parameter was perturbed. A first observation is that even without energy conduction, a steady burning flame is be obtained at all three equivalence ratios.This is attributed to the upstream diffusion of radicals and other reactive species. Yet, in each case the steady flame is pushed significantly closer to the stagnation plane in the absence of of energy conduction, indicating a weakening of the flame. As suggested by defining Lewis number based on the limiting reactant, under lean conditions the flame extinguishes with the elimination of methane diffusion and under rich conditions the flame extinguishes with the elimination of oxygen diffusion. Interestingly, under stoichiometric conditions, the elimination of oxygen diffusion extinguishes the flame, but the elimination of methane diffusion does not, though it does show a strong weakening effect on the flame. This observation is ascribed to the importance of O_2 in the key branching reaction $H + O_2 \rightleftharpoons O + OH$ and the steeper concentration gradient when going from inlet concentration to no remaining O_2. Though not shown in Figure 7, increases in λ are observed to extinguish the flame as too much thermal energy is lost and eliminating the diffusion of the major products, CO_2 and H_2O, is observed to have only small impact on the strained flame. However, a more interesting result is obtained when eliminating hydrogen radical diffusion leading to a strong weakening effect in both stoichiometric and rich conditions. While the observed impact of removing energy conduction established its importance in governing the propagation of the flame, this result demonstrates an importance of similar magnitude for the upstream propagation of key radicals. Energy conduction alone does not govern the propagation of the flame.

Across all equivalence ratios, methane flames are predicted to have Lewis numbers close to 1 with limited variability [75] making it a non-ideal fuel for further Lewis number investigations which do not artificially manipulate Le as was done in the study summarized in Figure 7. Therefore, propane, a convenient fuel used in many studies by Law and coworkers [15, 17, 21], is used instead. In the lean limit, propane tends to a Lewis number of 1.83 and in the rich limit to 0.93 [1]. To exhibit the capabilities of Ember with complex kinetic models, AramcoMech 1.3 is used here for analysis of lean and rich, strained propane flames. Figure 8 shows the results for $Le > 1$ where energy conduction exceeds propane diffusion toward the flame. As strain is systematically increased toward extinction, the flame moves closer to the stagnation plane, the peak flame temperature falls, and the peak reaction rate falls. The mass fractions of both CO_2 and H_2O at the stagnation plane trend down from their equilibrium values, signifying incomplete reactions. These trends are in agreement with the trends shown by Law (Figure 11) [1, 76]. However, while the CO_2 and H_2O mass

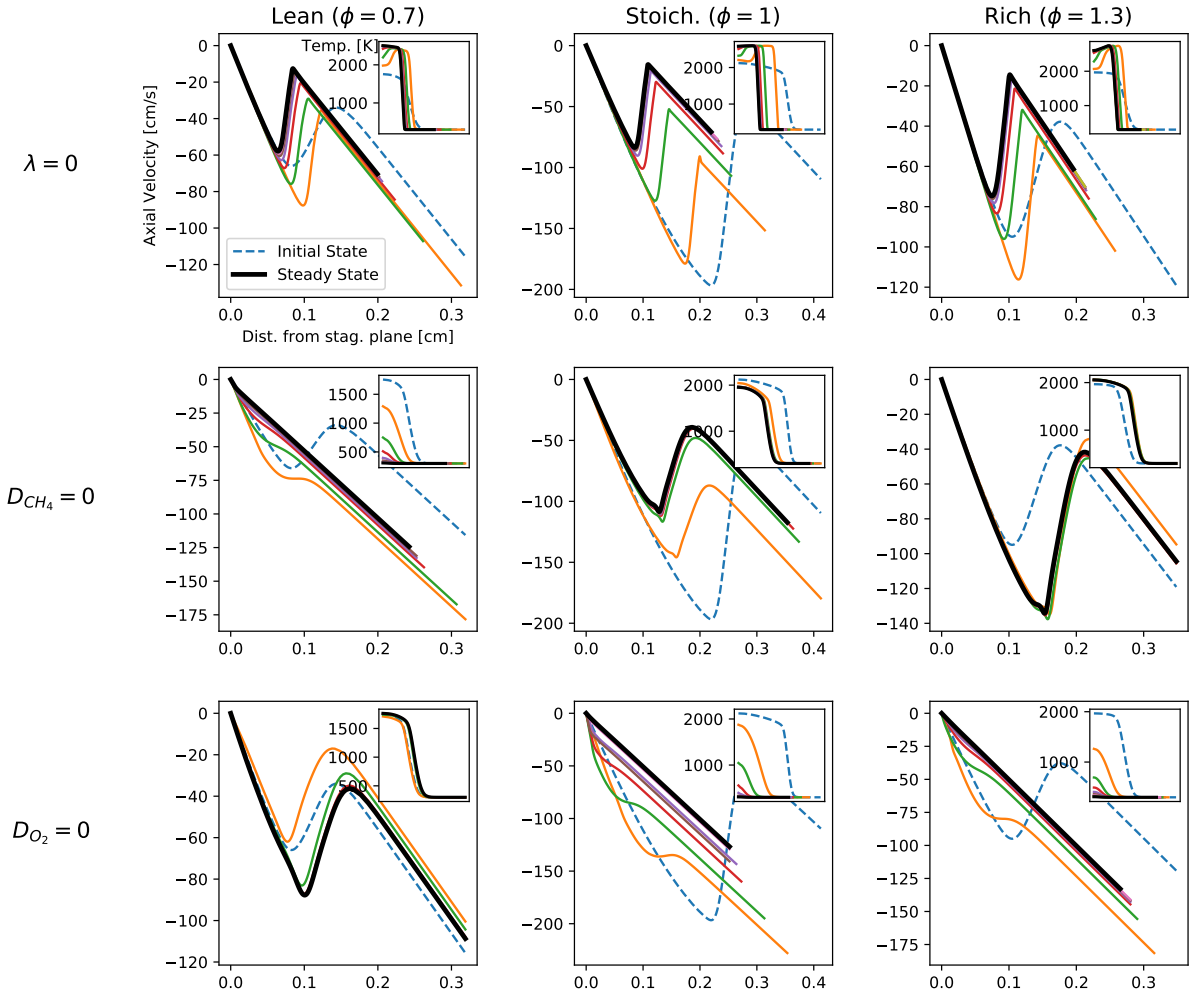

Figure 7: An investigation of Lewis number effects using complex chemistry simulations through elimination of fuel and oxidizer species diffusivities or elimination of energy conduction ($\lambda = 0$). This analysis was done using stoichiometric methane flames with a strain of 500 s^{-1} in Ember. FFCM1 is used as the kinetic model. Perturbations are achieved by first solving to steady state, then setting the specified diffusion parameter to 0 and allowing the system to progress in time to the new steady state.

fractions seem to indicate an incomplete reaction, Law characterizes this as an extinction with complete reaction. Looking at the reaction rate curves in Figure 8 the spike in reaction heat release is observed to be complete before the stagnation plane even at extinction, in accord with the prediction of Law [1], but secondary reactions have clearly not yet concluded their progression towards equilibrium. This is an example where multistep chemistry gives a somewhat different result than simple one-step-chemistry flame models.

For the rich conditions, Figure 9, results in accord with predictions by Law [1] are also observed. For very low strain rates, max temperature rises above the adiabatic flame temperature for the inlet composition and the peak reactivity also rises with increases in hydrodynamic strain. Very near the extinction point, the boundary limitation of the stagnation plane and incompleteness of reaction take over and ultimately force the peak reactivity of the strained flame to decrease immediately before extinction. What preliminarily appears to be an nonphysical result is observed for the mass fraction of CO_2 which rises with strain to a value well above its predicted equilibrium value based on the composition of the initial mixture. However, when this result is observed in connection with the full equilibrium profiles as functions of equivalence ratio shown in Figure 10, an explanation arises that increasing strain enhances the preferential diffusion of oxygen with respect to the rate of energy conduction/propagation of the flame effectively pushing the equivalence ratio back toward 1 from the starting value of 1.5. Law explains these results using a theoretical model of a streamline tube which expands in diameter as it approaches the stagnation plane. Law argues that since thermal and species diffusions are purely perpendicular to the stagnation plane, the change in cross-sectional area of the stream tube allows for additional supply of fuel/oxidizer from the surrounding flow when $Le < 1$ and further loss of thermal energy when $Le > 1$ [1].

The computed ESR values can be compared with the experimental values obtained by Law et al. [17]. The experimental value for finite boundary ESR at an equivalence ratio of 0.8 is interpolated to be about 830 s^{-1} while at an equivalence ratio of 1.5 the experimental value is 1090 s^{-1}. The infinite boundary ESR values calculated by Ember (Fig.8 & 9) are 1120 s^{-1} and 1220 s^{-1} respectively. Calculating percent difference with respect to the experimental value, the lean value differs by 35% and rich by 12%. The exact burner separation distances (BSDs) are not specified in [17]. However, an approximate range of BSDs are reported as 7 mm to 30 mm. In another work by the authors and coworkers, it is observed that the critical flame at extinction is independent of the the simulation BSD [69]. Solving Eq. 5 analytically for invicid and non-reacting flow before the flame yields

$$v_{axial} = v_{ax,0} - \frac{a^2}{4v_{ax,0}} z^2 \tag{41}$$

assuming an ideal plug flow burner without an initial velocity gradient. The strain constant is a, the initial plug flow velocity is $v_{ax,0}$, and the distance from the burner outlet is z. Knowing the value of a at extinction and an axial velocity point before the flame from the Ember solution, it is possible to use Eq. 41 to solve for the theoretical plug flow initial velocity, and thus approximate the ESR value for a finite boundary solution. Using the minimum value of the reported BSD range, the finite boundary ESR approximation for the lean propane is 929 s^{-1} and rich propane becomes 1150 s^{-1}. Both are overestimates of the corresponding experimental values, but are in significantly better agreement with the lean value now differing by only 12% from simulated to experimental value and the rich value by

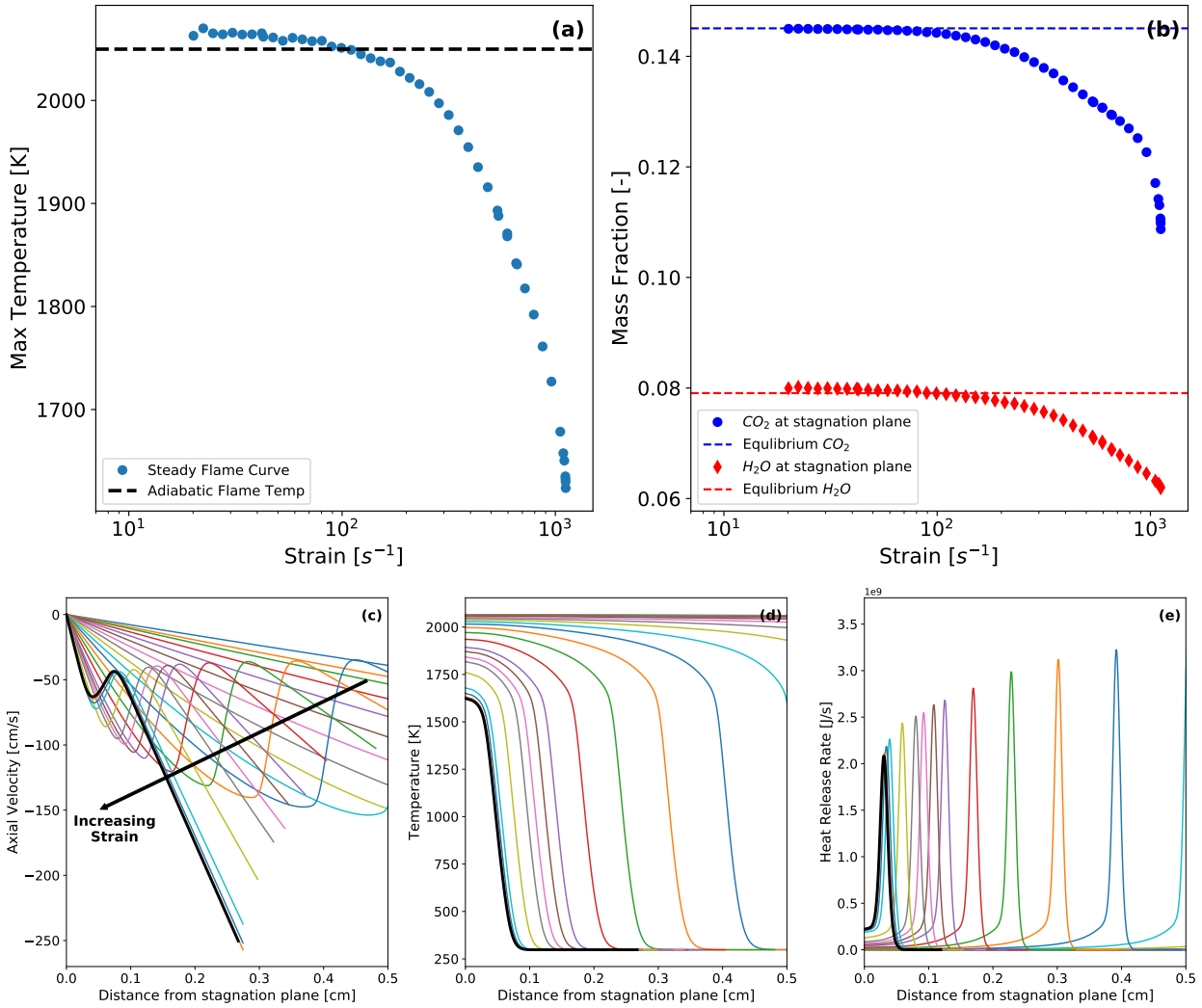

Figure 8: Extinction progression for a propane mixture of equivalence ratio 0.8, yielding a Lewis number greater than 1. AramcoMech 2.0 used.

5.6%. The remaining differences are likely attributed to uncertainties in the the kinetic model parameters and to a lesser degree error introduced by using the more computationally efficient mixture averaged transport formulation as opposed to the full multicomponent formulation including the thermal diffusion coefficients. Non-idealities in the experimental flow field might also contribute to the remaining differences.

4. Conclusions

In this work, Ember, a new, open-source, transient solver, has been introduced for the simulation of one-dimensional, strained flames. Through use of rebalanced Strang splitting, tailored differential equation solvers for each split calculation, and parallelization, Ember significantly outperforms conventional software such as Chemkin, typically used for such combustion simulations in terms of computation time. In the determination of extinction strain rate (ESR), Ember's computation time scales according to number of species to the

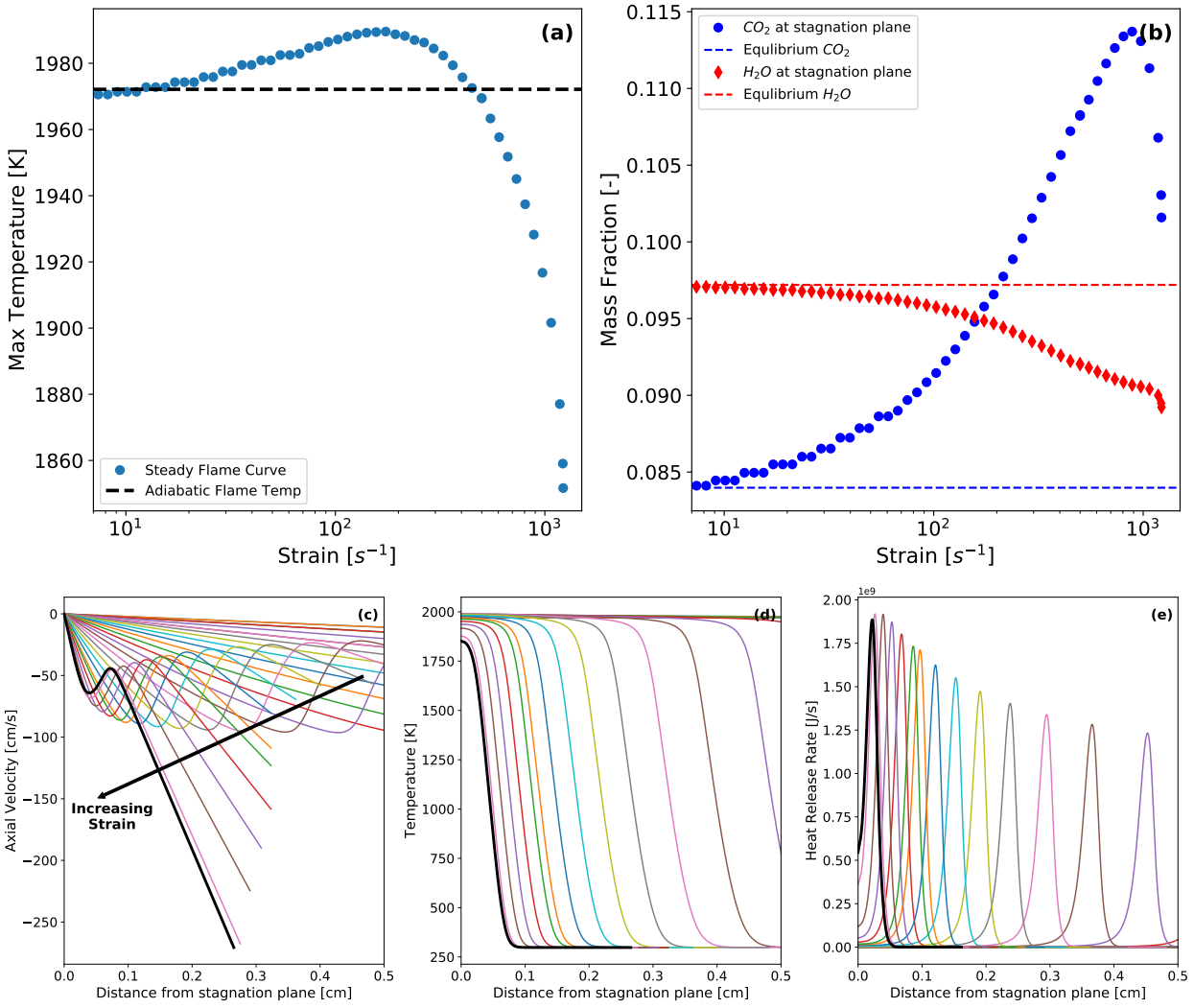

Figure 9: Extinction progression for a propane mixture of equivalence ratio 1.5, yielding a Lewis number less than 1. AramcoMech 2.0 used.

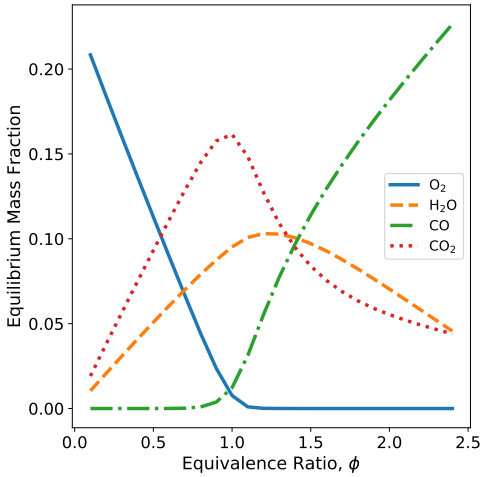

Figure 10: Equilibrium mixture for starting equivalence ratios of propane/air gas mixtures. Nitrogen and minor species are omitted for clarity.

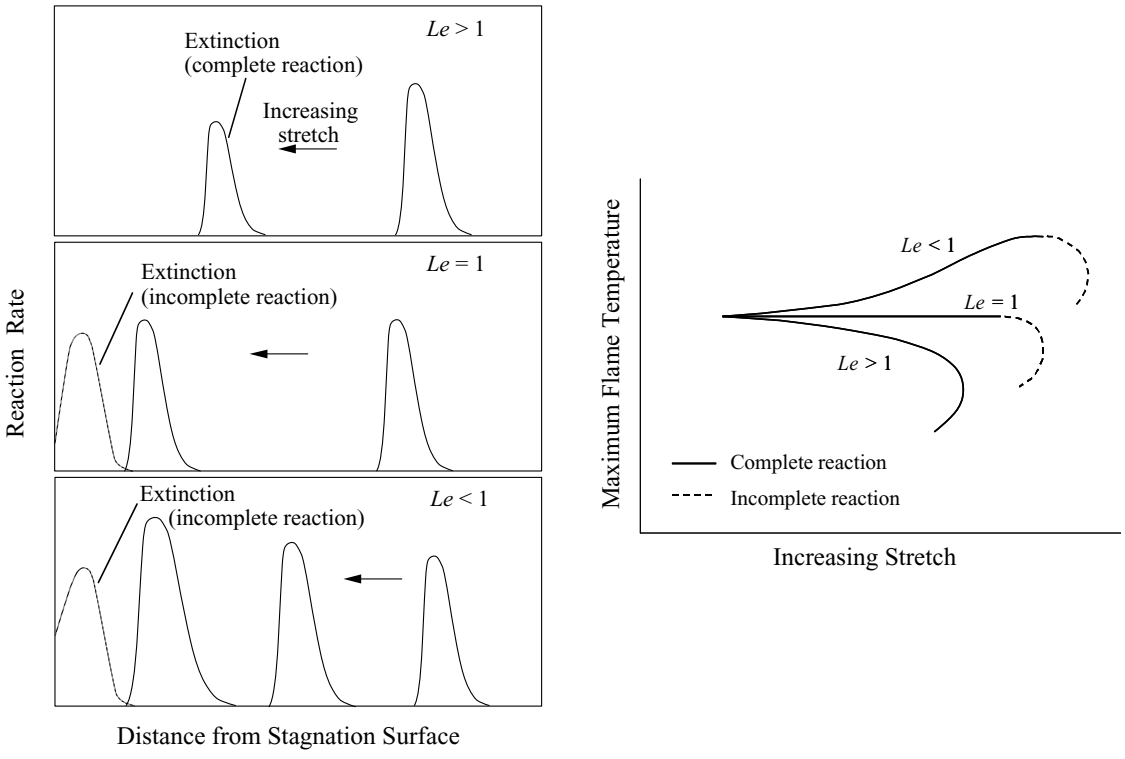

Figure 11: Theoretical Lewis number predictions included in *Combustion Physics* [1] for peak reactivity (Left) and progression to extinction (Right). Reproduced with permission from Cambridge University Press.

1.2 power while Chemkin-Pro 17.0 is observed to scale with species to the 2.9 power. This significant improvement in scaling of computation time allows for practical ESR calculations using large kinetic models such as AramcoMech 2.0 (493 species) which would otherwise not have been feasible. This is an important capability as increasingly complex fuel blends are investigated, requiring large, detailed kinetic models. For demonstration of the capabilities of Ember, it has been used to analyze the Lewis number trends predicted by asymptotic analyses of strained flames [1]. The transient solver capabilities of Ember were leveraged for an analysis of initially steady methane flames under lean, stoichiometric, and rich conditions for which the the energy conduction and individual species diffusions could instantaneously be perturbed and the strained flame allowed to relax to the new steady state. Of particular interest was the observed steady flame in the complete absence of energy conduction (Le=0), propagating through radical and species diffusion alone. Calculations with AramcoMech 2.0 demonstrated the capabilities of Ember with large detailed kinetic models and confirmed the Lewis number trends predicted by Law's asymptotic analyses hold even when the fuel chemistry is extremely complicated. A Lewis number less than one produced a growing peak reaction rate with increasing strain as additional fuel/oxidizer is diffusively supplied faster than the thermal propagation of the flame. Alternatively, a Lewis number greater than one yielded a flame with a steadily decreasing peak reaction rate as increasing strain enhances thermal energy losses from the flame. Though capable of very rapidly calculating extinction strain rate under ideal potential flow conditions as demonstrated in this work, Ember, as of yet cannot produce extinction strain rate predictions for conditions under which the finite boundary has significant impact. However, a new method of approximating the finite boundary ESR is introduced and demonstrated. Using this method, the simulated rich propane/air ESR differs by only 6% when compared with a previously reported experimental value.

5. Acknowledgments

AEL and WHG gratefully acknowledge financial support from ExxonMobil.

6. References

[1] C. K. Law, Combustion Physics, volume 14, Cambridge University Press, New York, 1st edition, 2006.

[2] C. K. Law, Asymptotic theory for ignition and extinction in droplet burning, Combustion and Flame 24 (1975) 89–98.

[3] ANSYS Inc., ANSYS 17.0 Chemkin-Pro Theory Manual, 2016.

[4] D. G. Goodwin, H. K. Moffat, R. L. Speth, Cantera: An object-oriented software toolkit for chemical kinetics, thermodynamics, and transport processes, `http://www.cantera.org`, 2017. Version 2.3.0.

[5] H. Pitsch, Flamemaster, a C++ computer program for 0D combustion and 1D laminar flame calculations, 1998.

[6] L. N. Trefethen, D. Bau, Numerical Linear Algebra, Society for Industrial and Applied Mathematics, Philadelphia, 1997.

[7] Y. Saad, Iterative methods for sparse linear systems, SIAM, 2003.

[8] T. A. Davis, Direct methods for sparse linear systems, SIAM, 2006.

[9] M. J. McNenly, R. A. Whitesides, D. L. Flowers, Faster solvers for large kinetic mechanisms using adaptive preconditioners, Proceedings of the Combustion Institute 35 (2015) 581–587.

[10] S. J. Shanbhogue, Y. S. Sanusi, S. Taamallah, M. A. Habib, E. M. A. Mokheimer, A. F. Ghoniem, Flame macrostructures, combustion instability and extinction strain scaling in swirl-stabilized premixed CH 4 /H 2 combustion, Combustion and Flame 163 (2015) 494–507.

[11] S. Taamallah, S. J. Shanbhogue, A. F. Ghoniem, Turbulent flame stabilization modes in premixed swirl combustion: Physical mechanism and Karlovitz number-based criterion, Combustion and Flame 166 (2016) 19–33.

[12] D. Michaels, S. J. Shanbhogue, A. F. Ghoniem, The impact of reactants composition and temperature on the flow structure in a wake stabilized laminar lean premixed CH4/H2/air flames; mechanism and scaling, Combustion and Flame 176 (2017) 151–161.

[13] C. K. Law, Deflagration and extinction of fuel droplet in a weakly-reactive atmosphere Deflagration and extinction of fuel droplet in a weakly- reactive atmosphere, The Journal of Chemical Physics 68 (1978).

[14] S. Ishizuka, C. K. Law, An experimental study on extinction and stability of stretched premixed flames, Symposium (International) on Combustion 19 (1982) 327–335.

[15] S. Ishizuka, K. Miyasaka, C. K. Law, Effects of heat loss, preferential diffusion, and flame stretch on flame-front instability and extinction of propane/air mixtures, Combustion and Flame 45 (1982) 293–308.

[16] S. H. Sohrab, C. K. Law, Extinction of premixed flames by stretch and radiative loss, International Journal of Heat and Mass Transfer 27 (1984) 291–300.

[17] C. K. Law, D. L. Zhu, G. Yu, Propagation and extinction of stretched premixed flames, Symposium (International) on Combustion 21 (1986) 1419–1426.

[18] P. Papas, I. Glassman, C. K. Law, K. Maruta, K. Abe, S. Hasegawa, S. Maruyama, J. Sato, Effects of Pressure and Dilution on the Extinction of Counterflow Nonpremixed Hydrogen-Air Flames, Lecture Notes in Physics Series 31 (1994) 147–156.

[19] J. S. Kistler, C. J. Sung, T. G. Kreut, C. K. Law, M. Nishioka, Extinction of counterflow diffusion flames under velocity oscillations, Symposium (International) on Combustion 26 (1996) 113–120.

[20] M. Nishioka, C. K. Law, T. Takeno, A flame-controlling continuation method for generating S-curve responses with detailed chemistry, Combustion and Flame 104 (1996) 328–342.

[21] C. K. Law, S. Ishizuka, M. Mizomoto, Lean-limit extinction of propane/air mixtures in the stagnation-point flow, Symposium (International) on Combustion 18 (1981) 1791–1798.

[22] S. H. Chung, J. S. Kim, C. K. Law, Extinction of interacting premixed flames: Theory and experimental comparisons, Symposium (International) on Combustion 21 (1986) 1845–1851.

[23] C. Sung, C. Law, Structural Sensitivity, Response, and Extinction of Unsteady Counterflow Flames, AIAA paper (1998) 98–0555.

[24] C. J. Sung, C. K. Law, Structural sensitivity, response, and extinction of diffusion and premixed flames in oscillating counterflow, Combustion and Flame 123 (2000) 375–388.

[25] E. W. Christiansen, S. D. Tse, C. K. Law, A computational study of oscillatory extinction of spherical diffusion flames, Combustion and Flame 134 (2003) 327–337.

[26] S. W. Yoo, E. W. Christiansen, C. K. Law, Oscillatory extinction of spherical diffusion flames: Micro-buoyancy experiment and computation, Proceedings of the Combustion Institute 29 (2002) 29–36.

[27] Y. L. Wang, P. S. Veloo, F. N. Egolfopoulos, T. T. Tsotsis, A comparative study on the extinction characteristics of non-premixed dimethyl ether and ethanol flames, Proceedings of the Combustion Institute 33 (2011) 1003–1010.

[28] Y. L. Wang, A. T. Holley, C. Ji, F. N. Egolfopoulos, T. T. Tsotsis, H. J. Curran, Propagation and extinction of premixed dimethyl-ether/air flames, Proceedings of the Combustion Institute 32 (2009) 1035–1042.

[29] C. Ji, E. Dames, Y. L. Wang, H. Wang, F. N. Egolfopoulos, Propagation and extinction of premixed C5-C12 n-alkane flames, Combustion and Flame 157 (2010) 277–287.

[30] C. Ji, R. Zhao, B. Li, F. N. Egolfopoulos, Propagation and extinction of cyclopentadiene flames, Proceedings of the Combustion Institute 34 (2013) 787–794.

[31] B. Li, N. Liu, R. Zhao, F. N. Egolfopoulos, H. Zhang, Extinction Studies of Flames of Heavy Neat Hydrocarbons and Practical Fuels, Journal of Propulsion and Power 29 (2013) 352–361.

[32] C. Ji, E. Dames, H. Wang, F. N. Egolfopoulos, Propagation and extinction of benzene and alkylated benzene flames, Combustion and Flame 159 (2012) 1070–1081.

[33] C. Vagelopoulos, F. Egolfopoulos, Laminar flame speeds and extinction strain rates of mixtures of carbon monoxide with hydrogen, methane, and air, Symposium (International) on Combustion 25 (1994) 1317–1323.

[34] B. Li, Y. Zhang, H. Zhang, F. N. Egolfopoulos, Extinction studies of non-premixed isocetane and decalin flames, Proceedings of the Combustion Institute 35 (2015) 965–972.

[35] O. Park, P. S. Veloo, H. Burbano, F. N. Egolfopoulos, Studies of premixed and non-premixed hydrogen flames, Combustion and Flame 162 (2015) 1078–1094.

[36] K. Seshadri, T. Lu, O. Herbinet, S. Humer, U. Niemann, W. J. Pitz, R. Seiser, C. K. Law, Experimental and kinetic modeling study of extinction and ignition of methyl decanoate in laminar non-premixed flows, Proceedings of the Combustion Institute 32 I (2009) 1067–1074.

[37] T. Bieleveld, A. Frassoldati, A. Cuoci, T. Faravelli, E. Ranzi, U. Niemann, K. Seshadri, Experimental and kinetic modeling study of combustion of gasoline, its surrogates and components in laminar non-premixed flows, Proceedings of the Combustion Institute 32 (2009) 493–500.

[38] S. Honnet, K. Seshadri, U. Niemann, N. Peters, A surrogate fuel for kerosene, Proceedings of the Combustion Institute 32 I (2009) 485–492.

[39] U. Niemann, R. Seiser, K. Seshadri, Ignition and extinction of low molecular weight esters in nonpremixed flows, Combustion Theory and Modelling 14 (2010) 875–891.

[40] S. M. Sarathy, S. Vranckx, K. Yasunaga, M. Mehl, P. Oßwald, W. K. Metcalfe, C. K. Westbrook, W. J. Pitz, K. Kohse-Höinghaus, R. X. Fernandes, H. J. Curran, A comprehensive chemical kinetic combustion model for the four butanol isomers, Combustion and Flame 159 (2012) 2028–2055.

[41] U. Niemann, K. Seshadri, F. A. Williams, Effect of pressure on structure and extinction of near-limit hydrogen counterflow diffusion flames, Proceedings of the Combustion Institute 34 (2013) 881–886.

[42] U. Niemann, K. Seshadri, F. A. Williams, Methane, ethane, and ethylene laminar counterflow diffusion flames at elevated pressures: Experimental and computational investigations up to 2.0MPa, Combustion and Flame 161 (2014) 138–146.

[43] A. Alfazazi, U. Niemann, H. Selim, R. J. Cattolica, S. M. Sarathy, Effects of Substitution on Counterflow Ignition and Extinction of C3 and C4 Alcohols, Energy and Fuels 30 (2016) 6091–6097.

[44] R. Seiser, H. Pitsch, K. Seshadri, W. J. Pitz, H. J. Curran, Extinction and autoignition of n-heptane in counterflow configuration, Proceedings of the Combustion Institute 28 (2000) 2029–2037.

[45] G. S. Jackson, R. Sai, J. M. Plaia, C. M. Boggs, K. T. Kiger, Influence of H2 on the response of lean premixed CH4 flames to high strained flows, Combustion and Flame 132 (2003) 503–511.

[46] S. H. Won, W. Sun, Y. Ju, Kinetic effects of toluene blending on the extinction limit of n-decane diffusion flames, Combustion and Flame 157 (2010) 411–420.

[47] A. Neagos, V. Bykov, U. Maas, Study of extinction limits of diluted hydrogen-air counter-flow diffusion flames with the redim method, in: Combustion Science and Technology, volume 186, pp. 1502–1516.

[48] R. K. Gehmlich, A. Kuo, K. Seshadri, Experimental investigations of the influence of pressure on critical extinction conditions of laminar nonpremixed flames burning condensed hydrocarbon fuels, jet fuels, and surrogates, Proceedings of the Combustion Institute 35 (2015) 937–943.

[49] R. J. Kee, F. M. Rupley, J. A. Miller, Chemkin-II: A Fortran chemical kinetics package for the analysis of gas-phase chemical kinetics, Technical Report, Sandia National Labs., Livermore, CA (USA), 1989.

[50] R. J. Kee, J. A. Miller, T. H. Jefferson, CHEMKIN: A general-purpose, problem-independent, transportable, FORTRAN chemical kinetics code package, Technical Report, Sandia National Labs., Livermore, CA (USA), 1980.

[51] R. J. Kee, F. M. Rupley, E. Meeks, J. A. Miller, CHEMKIN-III: A FORTRAN chemical kinetics package for the analysis of gas-phase chemical and plasma kinetics, Technical Report, Sandia National Labs., Livermore, CA (USA), 1996.

[52] R. J. Kee, J. A. Miller, G. H. Evans, G. Dixon-Lewis, A Computational Model of the Structure and Extinction of Strained, Opposed Flow, Premixed Methane-Air Flames, Proceedings of the Combustion Institute 22 (1988) 1479–1494.

[53] Y. Dong, A. T. Holley, M. G. Andac, F. N. Egolfopoulos, S. G. Davis, P. Middha, H. Wang, Extinction of premixed H2/air flames: Chemical kinetics and molecular diffusion effects, Combustion and Flame 142 (2005) 374–387.

[54] M. Mehl, W. J. Pitz, C. K. Westbrook, H. J. Curran, Kinetic modeling of gasoline surrogate components and mixtures under engine conditions, Proceedings of the Combustion Institute 33 (2011) 193–200.

[55] W. K. Metcalfe, S. M. Burke, S. S. Ahmed, H. J. Curran, A hierarchical and comparative kinetic modeling study of C1 - C2 hydrocarbon and oxygenated fuels, International Journal of Chemical Kinetics 45 (2013) 638–675.

[56] Y. Li, C. W. Zhou, K. P. Somers, K. Zhang, H. J. Curran, The oxidation of 2-butene: A high pressure ignition delay, kinetic modeling study and reactivity comparison with isobutene and 1-butene, Proceedings of the Combustion Institute 36 (2017) 403–411.

[57] C. W. Zhou, Y. Li, E. O'Connor, K. P. Somers, S. Thion, C. Keesee, O. Mathieu, E. L. Petersen, T. A. DeVerter, M. A. Oehlschlaeger, G. Kukkadapu, C. J. Sung, M. Alrefae, F. Khaled, A. Farooq, P. Dirrenberger, P. A. Glaude, F. Battin-Leclerc, J. Santner, Y. Ju, T. Held, F. M. Haas, F. L. Dryer, H. J. Curran, A comprehensive experimental and modeling study of isobutene oxidation, Combustion and Flame 167 (2016) 353–379.

[58] U. Burke, W. K. Metcalfe, S. M. Burke, K. A. Heufer, P. Dagaut, H. J. Curran, A detailed chemical kinetic modeling, ignition delay time and jet-stirred reactor study of methanol oxidation, Combustion and Flame 165 (2016) 125–136.

[59] S. Burke, U. Burke, R. Mc Donagh, O. Mathieu, I. Osorio, C. Keesee, A. Morones, E. L. Petersen, W. Wang, T. A. DeVerter, M. A. Oehlschlaeger, B. Rhodes, R. K. Hanson, D. F. Davidson, B. W. Weber, C.-J. Sung, J. S. Santner, Y. Ju, F. L. Dryer, E. N. Volkov, E. J. K. Nilsson, A. A. Konnov, M. Alrefae, F. Khaled, A. Farooq, P. Dirrenberger, P. A. Glaude, F. Battin-Leclerc, H. J. Curran, An experimental and modeling study of propene oxidation. Part 2: Ignition delay time and flame speed measurements, Combustion and Flame 162 (2015) 296–314.

[60] S. M. Burke, W. Metcalfe, O. Herbinet, F. Battin-Leclerc, F. M. Haas, J. Santner, F. L. Dryer, H. J. Curran, An experimental and modeling study of propene oxidation. Part 1: Speciation measurements in jet-stirred and flow reactors, Combustion and Flame 161 (2014) 2765–2784.

[61] A. Kéromnès, W. K. Metcalfe, K. A. Heufer, N. Donohoe, A. K. Das, C.-J. Sung, J. Herzler, C. Naumann, P. Griebel, O. Mathieu, M. C. Krejci, E. L. Petersen, W. J. Pitz, H. J. Curran, An experimental and detailed chemical kinetic modeling study of hydrogen and syngas mixture oxidation at elevated pressures, Combustion and Flame 160 (2013) 995–1011.

[62] C. W. Gao, J. W. Allen, W. H. Green, R. H. West, Reaction Mechanism Generator: Automatic construction of chemical kinetic mechanisms, Computer Physics Communications 203 (2016) 212–225.

[63] F. Seyedzadeh Khanshan, R. H. West, Developing detailed kinetic models of syngas production from bio-oil gasification using Reaction Mechanism Generator (RMG), Fuel 163 (2016) 25–33.

[64] R. L. Speth, Ember: A quasi-one-dimensional, unsteady flame solver, https://doi.org/10.5281/zenodo.1004753, 2017. Version 1.4.0.

[65] R. L. Speth, W. H. Green, S. MacNamara, G. Strang, Balanced Splitting and Rebalanced Splitting, SIAM Journal on Numerical Analysis 51 (2013) 3084–3105.

[66] R. J. Kee, M. E. Coltrin, P. Glarborg, Chemically Reacting Flow: Theory & Practice, John Wiley & Sons, Inc., Hoboken, 1st edition, 2003.

[67] A. C. Hindmarsh, P. N. Brown, K. E. Grant, S. L. Lee, R. Serban, D. E. Shumaker, C. S. Woodward, SUNDIALS: Suite of nonlinear and differential/algebraic equation solvers, ACM Transactions on Mathematical Software (TOMS) 31 (2005) 363–396.

[68] D. R. Mott, E. S. Oran, B. van Leer, A quasi-steady-state solver for the stiff ordinary differential equations of reaction kinetics, Journal of Computational Physics 164 (2000) 407 – 428.

[69] A. E. Long, H. Burbano, R. L. Speth, A. Movaghar, F. N. Egolfopoulos, W. H. Green, An apparatus-independent extinction strain rate in counterflow flames, Proceedings of the Combustion Institute (Submitted).

[70] G. P. Smith, Y. Tao, H. Wang, Foundational Fuel Chemistry Model Version1.0 (FFCM-1), http://nanoenergy.stanford.edu/ffcm1, 2016.

[71] D. Chen, K. Wang, H. Wang, Violation of collision limit in recently published reaction models, Combustion and Flame 186 (2017) 208 – 210.

[72] ANSYS Inc., CHEMKIN-PRO 17.0, 2016.

[73] G. P. Smith, D. M. Golden, M. Frenklach, N. W. Miriaty, B. Eiteneer, M. Goldenberg, T. Bowman, R. K. Hanson, S. Song, W. C. Gardiner, V. Lissianski, Z. Qin, GRImech3.0, http://www.me.berkeley.edu/gri_mech/, 2000.

[74] H. Wang, X. You, A. Joshi, S. Davis, A. Laskin, F. Egolfopoulos, C. Law, U. M. Version II, High-temperature combustion reaction model of h 2/co/c 1–c 4 compounds, http://www.ignis.usc.edu/USC_Mech_II.htm, 2000.

[75] D. Lapalme, R. Lemaire, P. Seers, Assessment of the method for calculating the Lewis number of H 2 /CO/CH 4 mixtures and comparison with experimental results, International Journal of Hydrogen Energy 42 (2017) 8314–8328.

[76] C. K. Law, Dynamics of stretched flames, Symposium (International) on Combustion 22 (1989) 1381–1402.